Arabidopsis *TITAN LIKE* is required for U12-type intron splicing, especially for AT–AC subtypes

Tomoko Niwa[1, 2], Junshin Miyamoto[3], Haruka Iwai[3], Takaaki Kojima[4], and Takamasa Suzuki[3*]

[1]Department of Agricultural Chemistry, School of Agriculture, Meiji University, 1-1-1 Higashi-Mita, Tama-ku, Kawasaki, Kanagawa, 214-8571, Japan

[2]Organization for the Strategic Coordination of Research and Intellectual Properties, Meiji University, 1-1-1 Higashi-Mita, Tama-ku, Kawasaki, Kanagawa, 214-8571, Japan

[3]Department of Biological Chemistry, College of Bioscience and Biotechnology, Chubu University, 1200 Matsumoto-cho, Kasugai, Aichi 487-8501, Japan

[4]Department of Agrobiological Resources, Faculty of Agriculture, Meijo University, 1-501 Shiogamaguchi, Tempaku-ku, Nagoya 468-8502, Japan

Corresponding author

*Takamasa Suzuki, email: takamasa@tsbio.info

Abstract

Many eukaryotes have two types of spliceosome, i.e., the U2-dependent and U12-dependent spliceosomes. The terminal dinucleotides of almost all introns spliced by the U2-dependent spliceosome are GT–AG, whereas the most of the rest involved the U12-dependent spliceosome ending in AT–AC. How the U12-dependent spliceosome splices two types of introns with different ends also remains poorly understood. For example, it has been reported that human CENATAC is a subunit of U12-dependent spliceosome and is—uniquely—required for the splicing of AT–AC introns. The Arabidopsis genome contains one gene called *TITAN LIKE* (*TTL*), a homolog of *CENATAC*, but the function this plays in splicing is unknown. In this paper we created a weak TTL mutant named *ttl-142*, and investigated the function of TTL during splicing. We found that *ttl-142* had a 14-residue deletion, and that homozygous mutants showed morphological abnormalities. Most U12-dependent introns were less spliced in *ttl-142* than in the wild type, and the splicing of AT–AC introns was particularly suppressed. Splicing suppression in *ttl-142* was more extensive than in a DROL1 mutant, which contains a mutation in a gene that is specifically required for AT–AC intron splicing. In contrast, fewer genes showed changes in expression levels in *ttl-142* than in *drol1*, and most DEGs in *ttl-142* and *drol1* were different. These results suggest that the phenotypes of *ttl-142* and *drol1* mutants may correspond to the impairment of specific spliceosomal functions.

Keywords

Arabidopsis thaliana, AT–AC intron, minor intron, splicing, *titan like,* TTL

Introduction

Many eukaryotes, including plants and vertebrates, possess two types of spliceosome (Turunen et al. 2013). One is the U2-dependent (major) spliceosome, which comprises five small nuclear RNAs (snRNAs) named U1, U2, U4, U5, and U6, as well as numerous other proteins (Wilkinson et al. 2019). The U2-dependent spliceosome is responsible for splicing nearly 99% of introns. The second type is the U12-dependent (minor) spliceosome, which consists of U11, U12, U4atac, U5, and U6atac snRNAs, combined with both unique proteins and several common to the U2-dependent spliceosome (Turunen et al. 2013; Ding et al. 2023). The introns spliced by each spliceosome exhibit different consensus sequences at their respective 5′ ends and branching point sequences and have been considered mutually exclusive. While the GT–AG sequences present at the ends of introns are highly conserved among eukaryotes, approximately one-third of U12-type introns, which are spliced by the U12-dependent spliceosome, contain an AT–AC sequence. It is unclear how the U12-dependent spliceosome splices two introns with different boundaries, but two protein subunits specific to the AT–AC intron—i.e., DROL1 and CENATAC—have recently been identified (Suzuki et al. 2022; de Wolf et al. 2021).

While screening for *Arabidopsis thaliana* mutants containing defects in the repression of seed-maturation genes, we identified the *defective repression of the OLE3:LUC 1* (*drol1*) mutant, which harbored a mutation in a splicing factor (Suzuki et al. 2018). The *A. thaliana* DROL1 protein was homologous to yeast DIB1 and human Dim1, two subunits of U5 snRNP, but belonged to a distinct subfamily (Suzuki et al. 2022). Moreover, a comprehensive transcriptomic analysis of the *drol1* mutant revealed that splicing of the AT–AC intron was specifically suppressed, suggesting that DROL1 is a splicing factor specific to AT–AC introns.

The Dim1 protein, together with PRP8, forms a binding pocket for 5′ splice sites in the B complex of the human U2-dependent spliceosome (Bertram et al. 2017; Zhan et al. 2018). In this complex, a 5′-terminal guanine stacks with the phenylalanine residue present in PRP8, and the uracil next to the guanine is located close to Dim1 (Bertram et al. 2017). Prior structural analyses have suggested that Dim1 plays a direct role during recognition of the 5′ splice site (Bertram et al. 2017). Dim2, an ortholog of DROL1, has also been identified within the human U12-dependent B complex (Bai et al. 2024). Although imaging resolution was low and the mechanism of the interaction between Dim2 and the 5′ splice site remains unclear, it may recognize the 5′ terminal AU as Dim1 does.

Another gene called *CENATAC* has been identified as a cause of human mosaic variegated aneuploidy (de Wolf et al. 2021). Originally, the CENATAC protein was reported to be a subunit of the U12-dependentt spliceosome since it coprecipitated with minor spliceosome-specific

proteins and the U4atac and U6atac snRNAs. Comprehensive transcriptome analysis of CENATAC-depleted cells revealed increased retention of U12-type introns, especially the AT–AC subtype. Taken together, these results indicate that CENATAC is required for the splicing of AT–AC introns, as for DROL1, although it is also required for some U12-type GT–AG introns.

More recently, CENATAC has also been identified in structural models of the U12-dependent spliceosomal B complex (Bai et al. 2024). There, it has been shown to bind to the 5′ cap of U4atac snRNA and to the loop of U6atac snRNA. Furthermore, CENATAC is not located adjacent to an intron, and it therefore remains unclear how this factor specifically acts on AT–AC introns.

The Arabidopsis ortholog of *CENATAC* has been named *TITAN LIKE* (*TTL*), since the mutant phenotype resembles the *titan* mutant by manifesting abnormalities in embryo development (Lu et al. 2012). *TTL* encodes a protein containing a C2H2 domain, but the mechanism by which its defect causes embryonic lethality remains unknown.

One interesting feature of the *CENATAC*/*TTL* gene family is that they contain a U12-type intron that cannot be spliced out to encode a functional protein (de Wolf et al. 2021). In vertebrates, *CENATAC* orthologs contain a U12-type intron with GT–AG termini that share a 3′ splice site with a U2-type intron. Thus, when spliced at the U12-type 5′ splice site, the translational frame of the next exon is shifted, resulting in a nonfunctional protein (de Wolf et al. 2021). In plants, *TTL* orthologs generally contain AT–AC introns within exons. Moreover, splicing of these introns can result in the loss of amino acid sequences, thereby also causing a frameshift (de Wolf et al. 2021; Lu et al. 2012). *TTL* undergoes alternative splicing to produce nine different transcripts, but only those retaining the AT–AC intron have been shown to complement the *ttl* mutant (Lu et al. 2012).

In this paper, we investigated the function of Arabidopsis TTL during splicing. To do so, we created a viable allele of TTL and obtained a mutant, named *ttl-142*, which contains a 42-nucleotide deletion in its first exon. The *ttl-142* mutant exhibited a weak morphological phenotype similar to *drol1*, but suppressed AT–AC intron splicing to a greater degree. Moreover, unlike *drol1*, the U12-type GT–AG intron was also less spliced in *ttl-142*. When compared with wild-type *A. thaliana*, we identified fewer DEGs in *ttl-142* than in *drol1*, a finding that is consistent with its morphological phenotype. Taken together, these results indicate that TTL, like CENATAC, is a splicing factor required for splicing of U12-type introns, especially AT–AC-type introns. Furthermore, we speculate that the phenotypes of *drol1* and *ttl-142* plants may depend in part on genetic defects caused by retention of AT–AC introns and in part on the disrupted splicing caused by each mutation.

Results and Discussion

ttl-142 *is a weak allele for* TITAN LIKE

First, to create Arabidopsis mutants for *TITAN LIKE* (*TTL*), we designed single guide RNAs (sgRNAs) that were subsequently introduced into Arabidopsis wild-type (WT) Col-0 plants. One transformant that received sgRNA1 was found to lack 42 nucleotides from the 1st exon of *TTL*, and this mutation was therefore named *ttl-142* (Figures 1A and B). Next, plants homozygous for *ttl-142* were phenotyped: they appeared to be smaller than WT plants and showed flattened cotyledons and dark green leaves (Figures 1C and D). Overall, these phenotypes were reminiscent of *drol1*, although *less* severe (Figure 1E).

To confirm that these phenotypes were caused by the *ttl-142* mutation, we introduced the DNA fragment for entire *TTL* gene—including 1 kbp upstream and 0.6 kbp downstream regions—into *ttl-142* plants. The resulting transformant showed a phenotype that was highly similar to the WT (Figure 1F), suggesting that the phenotypes observed for *ttl-142* were not caused by off-target mutations.

Next, we performed RNA-Seq and found that the *ttl-142* mutant expressed TTL mRNA containing a 42 bp deletion (Figure 2A). Our functional prediction indicated that this creates a TTL protein that lacks 14 amino acids. Moreover, this deletion is in the second of two C2H2-type zinc finger domains present in TTL. In a previous study of a model of the human minor spliceosome, the TTL homolog CENATAC used these two zinc fingers to bind to the 5′ cap of U4atac and the central stem loop of U6atac snRNAs (Figure S1, Bai et al. 2024). These results therefore suggest that the *ttl-142* mutation affects the binding of TTL to U4atac/U6atac di-snRNPs.

In addition to the C2H2 motif, the CENATAC/TTL gene family contains several other conserved motifs. Four motifs of unknown function (i.e., M1–M4) are conserved in the C-termini of metazoans (de Wolf et al. 2021), but *TTL* lacks a region that has high homology to M2 (Figure S1D). The mutation found in the human patient changed the splicing site, and resulted in the loss of M3 and M4 (de Wolf et al. 2021). This evidence suggests that M3 and M4 have an important function. In the three-dimensional structure predicted by AlphaFold3 (Abramson et al. 2024), these motifs are part of the α-helix, but cannot be identified in the current spliceosome model (Figures S1A and B). In the original *ttl* mutant, no mRNA was detected 5′ upstream of the T-DNA insertion site (Lu et al. 2012), so it is unclear which defect in which region causes lethality. Here, we report that the *ttl-142* mutation does not affect the amino acid sequence at the C-terminus (Figure S1C); moreover, it has a weaker phenotype than *ttl* and may be a viable allele. In future,

to better elucidate the function of *TTL*, it will be necessary to investigate the role this motif plays during splicing.

***RNA-Seq analysis of splicing in* ttl-142**

Next, RNA extracted from three-day-old *ttl-142* plants was subjected to RNA-Seq analysis. The resulting transcriptomic dataset from *ttl-142* was then compared to sequences from WT plants and the *drol1-1* mutant (Suzuki et al. 2022). Splicing patterns were analyzed by ASpli (Estefania et al. 2021), and the percentage of intron retention (PIR) was calculated. Figure 3A shows PIR comparisons among WT and *ttl-142* plants. Although most PIR values were similar between the WT and *ttl-142* mutant, 479 introns showed significant differences (FDR < 0.01; red and blue dots shown in Figure 3A). Of these, 60 introns (13%; red dots shown in Figure 3A) had nucleotide sequences that started with AT and ended with AC (i.e., putative AT–AC introns). Overall, this proportion of AT–AC introns was far greater than that found in the wider Arabidopsis genome (0.06%; $P < 2.2 \times 10^{-16}$ according to a chi-squared test). Moreover, among the 479 introns identified, the PIRs of half of non-AT–AC introns were significantly increased, while another half had decreased in *ttl-142* plants. In contrast, the PIRs of almost all AT–AC introns increased, indicating that splicing of AT–AC introns was specifically suppressed in the *ttl-142* mutant. Genes with AT–AC introns whose PIR was changed in *ttl-142* are shown in Table 1.

The splicing patterns of AT–AC introns were then compared between the *ttl-142* and *drol1-1* mutants (Figure 3B). Of the 79 AT–AC introns analyzed, 47 showed significant changes in PIR in both *ttl-142* and *drol1-1* mutants relative to the WT (FDR < 0.01; blue dots in Figure 3B). Here, the average difference in PIR was an increase of 9% in *ttl-142* ($P < 0.001$ according to a Student *t*-test). Eighteen AT–AC introns showed significantly increased PIR values only in *ttl-142* compared with WT (red squares in Figure 3B), but only one showed significantly increased PIR only in *drol1-1* (green triangle in Figure 3B). Taken together, these results indicate that splicing of AT–AC introns was more strongly suppressed in *ttl-142* mutants than in *drol1-1* mutants. This is inconsistent with the hypothesis that *ttl-142* has a weaker phenotype than *drol1-1* and suggests that the severe phenotype of *drol1-1* is not solely due to the inhibition of AT–AC intron splicing.

In general, AT–AC introns are spliced by the U12-dependent spliceosome, which also splices introns with a GT–AG dinucleotide terminus. Next we investigated the dependency of introns on the TTL for each type of intron. The U2-dependent spliceosome is the major spliceosome responsible for splicing of most introns. Here, and most of the PIRs of introns spliced by the U2-dependent spliceosome were zero or almost zero in both WT and *ttl-142* (Figure 3C, left column). Moreover, we observed no differences in the PIR values of U2-type introns between WT and *ttl-*

142 plants (Figure 3C, left bottom), suggesting that the TTL protein is not required for the U2-dependent spliceosome. The PIRs of most U12-type GT–AG introns were also zero in WT plants, but were larger in *ttl-142* plants (Figure 3C, middle column). Specifically, we observed that the difference in PIR for each intron was −24% on average, which was significantly different from zero ($P < 2.2 \times 10^{-16}$, Student *t*-test). Furthermore, the PIR values of U12-type AT–AC introns were significantly higher in *ttl-142* plants than in WT plants ($P < 2.2 \times 10^{-16}$, Student's *t*-test), with an average of −45% (Figure 3C right column). In *ttl-142* mutant plants, the PIR values of U12-type AT–AC introns were significantly greater than those of U12-type GT–AG introns ($P < 1.3 \times 10^{-8}$, Student's *t*-test). Taken together, these results indicate that TTL is required for U12-dependent intron splicing, particularly for AT–AC introns. This finding is consistent with prior results for human CENATAC, but differs from *drol1*, which is required only for the splicing of AT–AC introns.

Next, structural analysis of the human minor spliceosome has revealed that human CENATAC binds to the U4atac/U6atac di-snRNP (Bai et al. 2024). Previous biochemical analyses have also shown that CENATAC mainly binds to the U4atac/U6atac di-snRNP (de Wolf et al. 2021). These results are consistent with the fact that when CENATAC or TTL functions are impaired, all splicing of U12-type introns is suppressed. However, CENATAC is located far from the 5′ end of the intron in the spliceosome, and this cannot explain observed differences in dependency between U12-type GT–AG and AT–AC introns. In contrast, Dim1, a homolog of DROL1, is known to be in contact with the 5′ end of the intron (Bertram et al. 2017; Zhan et al. 2018). Functional analysis of DROL1 has shown that it regulates the specific binding of U5 snRNPs to the 5′ end of the intron (Suzuki et al., in preparation). However, further analysis is needed to clarify why U12-type AT–AC introns are more dependent on TTL.

RT-PCR analysis of AT–AC intron retention in ttl-142

Figure 2A presents compiled reads mapped to the *TTL* gene in WT and *ttl-142* mutant seedlings. Short reads obtained from WT seedlings mainly mapped to exons and not introns other than the fourth (Figure 2A, upper panel). Overall, *ttl-142* was similar to the WT except for the 42-nucleotide deletion in the first exon and the AT–AC intron in the third exon. The PIR for the AT–AC intron in the third exon was 44% in WT but 100% in *ttl-142*. This result was further confirmed by reverse transcriptase-assisted PCR (RT-PCR). RT-PCR was performed using primers designed upstream of the AT–AC intron and on exon 4 (Figure 2B). Both DNA fragments containing and not containing the AT–AC intron were detected in the WT (Figure 2C). However, when the same RT-PCR was performed on the *ttl-142* mutant, the peak for the DNA fragment containing only

the AT–AC intron was prominent, while the peak indicating the splicing of the AT–AC intron was barely visible (Figure 2D).

The *TTL* gene has an AT–AC intron in its third exon that encodes part of a functional protein. In WT strains, about half of TTL transcripts encode functional proteins, retaining the AT–AC intron, while the rest are spliced out. This balance may be maintained by a negative feedback loop, since TTL promotes splicing of the AT–AC intron. Here, our RNA-Seq dataset show that the amount of TTL transcript in *ttl-142* was approximately 2.4-fold higher than in the WT, which supports the possibility that TTL expression is regulated by negative feedback.

The histone deacetylase 2B (HD2B) gene is a member of the HD2 gene family, which encodes plant-specific histone deacetylase (Hollender and Liu 2008); moreover, its third intron is an AT–AC intron. In WT seedlings, all introns were fully spliced, but in *ttl-142*, 65% of the AT–AC introns remained (Figure 2E). In addition, DNA fragments containing AT–AC introns were absent from the transcriptome of WT, but they were significantly more abundant in *ttl-142*, as evidenced using RT-PCR (Figures 2G and H). Finally, we note that no significant differences were observed in the expression levels of HD2B between WT and *ttl-142*.

Differentially expressed genes in the* ttl-142 *mutant

Next, we compared genome-wide gene expression patterns between WT and *ttl-142* mutant plants. All short reads were aligned with the Arabidopsis cDNA and counted by transcript. These data were then analyzed using edgeR (Robinson et al. 2010) so we could identify and select differentially expressed genes (DEGs; FDR $< 1 \times 10^{-4}$). Compared with the WT, we identified 198 and 451 genes that were significantly up- and downregulated in *ttl-142* mutant plants, respectively (Figure 4, red squares and blue dots). Regarding *drol1-1*, we identified 792 and 1096 genes that were up- and downregulated compared to the WT, respectively (Figure 4, green triangles and blue dots). Overall, *drol1-1* had more DEGs than *ttl-142*, a fact that may explain the strength of its developmental phenotype; however this could not be explained by the degree of intron retention.

When comparing the *ttl-142* and *drol1-1* DEG datasets, we identified 36 genes that were upregulated and 169 genes that were downregulated in both (Figure 4, red squares). However, we also found 83 genes that showed opposing expression pattern changes in *ttl-142* and *drol1-1* plants (Figure 4, red squares), thereby indicating that the gene expression patterns of *ttl-142* and *drol1-1* are not similar.

Previous studies have reported that the gene ontology terms such as “lipid storage,” “response to abscisic acid,” “response to water deprivation,” and “response to salt stress” are

overrepresented in genes whose expression is higher in *drol1* relative to WT plants, while "mitotic cell cycle transition" and "regulation of cyclin-dependent protein serine/threonine kinase activity" are underrepresented (Suzuki et al. 2022). Here, we performed a similar analysis for *ttl-142*, and identified no significantly enriched ontologies in genes whose expression levels had either increased or decreased. Moreover, no significantly enriched ontologies were identified among genes whose expression levels were increased or decreased in both *drol1* and *ttl-142*. Taken together, these results indicate that increased expression of ABA-related genes and decreased expression of genes related to cell division in *drol1* are phenomena specific to that mutant and are not necessarily related to the inhibition of splicing of AT–AC introns.

Although *drol1* and *ttl-142* generate similar phenotypes in terms of cotyledon shape and leaf color, *drol1* is more severe (Figure 1). To date, it was thought that the phenotype of *drol1* was caused by splicing suppression specific to AT–AC introns (Suzuki et al. 2022). However, the phenotype of *ttl-142* in which splicing is suppressed to a greater degree than in *drol1* plants, showed a weaker phenotype. This indicates that the *drol1* phenotype cannot be explained by splicing suppression alone. In addition, *drol1* was shown to be highly sensitive to ABA, with the expression of genes related to ABA pathways significantly upregulated relative to the WT (Suzuki et al. 2022). Taken together, these findings suggest that the loss of DROL1 specifically inhibits some stage of splicing, and that this activates the ABA response.

Subcellular localization of the TTL protein

Next, we performed subcellular localization experiments to obtain localization information for the TTL protein. To do so, we first amplified a DNA fragment containing the full coding region for TTL from the Arabidopsis genome, fused it to GFP at its C-terminus, and placed it downstream of the 35S promoter. This recombinant gene was then introduced into Arabidopsis; however, no GFP fluorescence was observed (data not shown). We speculated that alternative splicing of the AT–AC intron decreases the abundance of transcripts encoding a functional TTL protein; thus, we introduced 23 base substitutions into the AT–AC intron without changing its amino acid sequence. The resulting modified gene was named TTLmmI (Figure S2). When GFP was linked to this TTLmmI and introduced, we observed a strong GFP signal (Figure 5). GFP was found to be localized in the nucleus, which is consistent with previous results using protoplasts (Lu et al. 2012). In some nuclei, the fluorescence was distributed unevenly, with some pictures revealing circular areas of intense fluorescence (Figure 5D insets). It has been proposed that snRNP biogenesis occurs in nucleoli and Cajal bodies (Ohtani, 2018), and that splicing occurs in nuclear speckles (Gordon et al. 2021). These observations may reflect the various states of TTL,

since its location may vary when it is either associated with U4atac/U6atac di-snRNPs or detached from the spliceosome.

Since the expression of mRNA for *TTL* was increased in *ttl-142* mutants, we suggested that the amount of TTL expression may be regulated by a negative feedback loop (de Wolf et al. 2021). Furthermore, GFP fused to TTL was not expressed in transformants, but GFP was observed when a mutation was introduced to the AT–AC intron. Since the AT–AC intron within the TTL exon encodes a portion of a functional protein and that TTL promotes splicing of the AT–AC intron, we suggested that the amount of TTL protein is regulated by a negative feedback loop mediated by the splicing of AT–AC introns. Such expression regulation by splicing factors may be a common feature of the CENATAC/TTL gene family.

Materials and Methods

Plant material and growth conditions

A. thaliana (L.) Heynh. strain Columbia (Col-0) were used as WT plants. *drol1-1* mutants were characterized previously (Suzuki et al. 2018). Unless otherwise indicated, seeds were first sterilized on 0.3% (w/v) gellan gum plates containing half-strength Murashige and Skoog medium (Wako, Japan) supplemented with 2% (w/v) sucrose, 0.05% (w/v) 2-morpholinoethanesulfonic acid (MES) (adjusted to pH 5.7 with KOH), 100 mg/L myo-inositol, 10 mg/L thiamine hydrochloride, 1 mg/L nicotinic acid, and 1 mg/L pyridoxine hydrochloride. Plant growth conditions were described in a previous study (Suzuki et al. 2018)

Gene cloning and plasmid construction

Next, we prepared gene editing constructs using pKI1.1R and combinations of specific oligo nucleotides (Tsutsui and Higashiyama 2016). Briefly, DNA fragments for the *TTL* gene were first amplified using the attB1_TTLp and attB2_TTLt primers and genomic DNA from Arabidopsis. Fragments were first ligated with pDONR, which was then amplified with attL1 and attL2 primers using an In-Fusion Cloning Kit (Takara, Tokyo, Japan). The obtained plasmid was named pDONR-TTLg. Inserts were then transferred into pFAST-G01 (Shimada et al. 2010) by LR reaction using Gateway cloning (Thermo Fisher Scientific, MA, USA); these were used for the complementation test as well as for transformation. Next, DNA fragments for the expression of GFP-fused TTL were amplified using attB1_TTL and attB2_TTL primers from pDONR-TTLg and were then cloned into pDONR as described above. Subsequently, the obtained plasmid was used for inverse PCR using TTL_mIS and TTL_mIA primers, and the resulting PCR product was circulated using an In-Fusion Cloning Kit. Finally, inserts were transferred into a pGWB550

binary vector (Nakagawa et al. 2007) then used for transformation. All oligonucleotides used in this experiment are listed in Table S1.

RNA extraction

Prior to RNA extraction, all plants were grown as per a previously described protocol (Suzuki et al. 2022). For all samples, total RNA was extracted from a frozen powder using a NucleoSpin RNA Plant Kit (Takara).

RNA-Seq analysis

For RNA-Seq, library preparation and sequencing were performed as previously described (Suzuki et al. 2022). Data analysis of RNA-Seq results was also performed as previously described (Suzuki et al. 2022).

RT-PCR and chip electrophoresis

For RT-PCR, cDNA was first reverse transcribed from 400 ng of total RNA using 100 U of SuperScript III (Thermo Fisher Scientific, MA, USA) and 1 pmol of each of the five antisense primers in a 10 µl volume. The resulting synthesized cDNA was the amplified by PCR using MightyAmp over 30 cycles before being analyzed using a MultiNA microchip electrophoresis platform (Shimadzu, Kyoto, Japan) after a fivefold dilution with water. All primers used are listed in Table S1.

Statistical analyses

All statistical tests in this study were performed using R version 4.3.3 (https://www.r-project.org/). Specifically, we used the t.test and chisq.test functions for Student's t-tests and chi-square tests, respectively.

Data Availability

The data underlying this article are available in DNA Data Bank of Japan, and can be accessed with accession No. PRJDB20300. Data for WT and *drol1* were obtained using accession No. PRJDB9966

Funding

This work was supported by a grant from JSPS KAKENHI (No. 23K05809 to T.S.), two grants from MEXT KAKENHI (Nos. JP20H05905 and JP20H05906 to T.S.), and two additional grants from Chubu University (Nos. 21M04A1 and 22210K to T.S.).

Acknowledgments

We thank Ayami Furuta and Mine Morimoto for valuable technical assistance. The authors would like to thank Enago (www.enago.jp) for English language review.

Author contributions

T.S. conceived the study; T.S. and T.N. designed the experiments; T.S., T.N., M.J., I.H., and T.K. carried out the experiments; T.S. analyzed the data; T.S. wrote the paper.

Disclosures/Conflicts of Interest

The authors declare that they have no conflicts of interest to disclose.

References

Abramson, J., Adler, J., Dunger, J., Evans, R., Green, T., Pritzel, A., et al. (2024) Accurate structure prediction of biomolecular interactions with AlphaFold 3. Nature 630: 493-500. https://doi.org/10.1038/s41586-024-07487-w.

Bai, R., Yuan, M., Zhang, P., Luo, T., Shi, Y. and Wan, R. (2024) Structural basis of U12-type intron engagement by the fully assembled human minor spliceosome. Science 383: 1245-1252. https://doi.org/10.1126/science.adn7272.

Bertram, K., Agafonov, D.E., Dybkov, O., Haselbach, D., Leelaram, M.N., Will, C.L., et al. (2017) Cryo-EM structure of a pre-catalytic human spliceosome primed for activation. Cell 170: 701-713.e11. https://doi.org/10.1016/j.cell.2017.07.011.

de Wolf, B., Oghabian, A., Akinyi, M.V., Hanks, S., Tromer, E.C., van Hooff, J.J.E., et al. (2021) Chromosomal instability by mutations in the novel minor spliceosome component *CENATAC*. EMBO J. 40: e106536. https://doi.org/10.15252/embj.2020106536.

Ding, Z., Meng, Y.R., Fan, Y.J. and Xu, Y.Z. (2023) Roles of minor spliceosome in intron recognition and the convergence with the better understood major spliceosome. Wiley Interdiscip. Rev. RNA 14: e1761. https://doi.org/10.1002/wrna.1761.

Estefania, M., Andres, R., Javier, I., Marcelo, Y. and Ariel, C. (2021) ASpli: integrative analysis of splicing landscapes through RNA-Seq assays Bioinformatics 37: 2609-2616.

Gordon, J.M., Phizicky, D.V. and Neugebauer, K.M. (2021) Nuclear mechanisms of gene expression control: pre-mRNA splicing as a life or death decision. Curr. Opin. Genet. Dev. 67: 67-76. https://doi.org/10.1016/j.gde.2020.11.002.

Hollender, C. and Liu, Z. (2008) Histone deacetylase genes in *Arabidopsis* development. J. Integr. Plant Biol. 50: 875-885. https://doi.org/10.1111/j.1744-7909.2008.00704.x.

Lu, X., Li, Y., Su, Y., Liang, Q., Meng, H., Li, S., et al. (2012) An Arabidopsis gene encoding a C2H2-domain protein with alternatively spliced transcripts is essential for endosperm development. J. Exp. Bot. 63: 5935-5944. https://doi.org/10.1093/jxb/ers243.

Nakagawa, T., Suzuki, T., Murata, S., Nakamura, S., Hino, T., Maeo, K., et al. (2007) Improved Gateway binary vectors: high-performance vectors for creation of fusion constructs in transgenic analysis of plants. Biosci. Biotechnol. Biochem. 71: 2095-2100. https://doi.org/10.1271/bbb.70216.

Ohtani, M. (2017) Plant snRNP biogenesis: a perspective from the nucleolus and Cajal bodies. Front. Plant Sci. 8: 2184. https://doi.org/10.3389/fpls.2017.02184.

Robinson, M.D., McCarthy, D.J. and Smyth, G.K. (2010) edgeR: a Bioconductor package for differential expression analysis of digital gene expression data. Bioinformatics 26: 139-140. https://doi.org/10.1093/bioinformatics/btp616.

Shimada, T.L., Shimada, T. and Hara-Nishimura, I. (2010) A rapid and non-destructive screenable marker, FAST, for identifying transformed seeds of *Arabidopsis thaliana*. Plant J. 61: 519-528. https://doi.org/10.1111/j.1365-313X.2009.04060.x.

Suzuki, T., Kawai, T., Takemura, S., Nishiwaki, M., Suzuki, T., Nakamura, K., et al. (2018) Development of the Mitsucal computer system to identify causal mutation with a high-throughput sequencer. Plant Reprod. 31: 117-128. https://doi.org/10.1007/s00497-018-0331-8.

Suzuki, T., Shinagawa, T., Niwa, T., Akeda, H., Hashimoto, S., Tanaka, H., et al. (2022) The *DROL1* subunit of U5 snRNP in the spliceosome is specifically required to splice AT–AC-type introns in *Arabidopsis*. Plant J. 109: 633-648. https://doi.org/10.1111/tpj.15582.

Tsutsui, H. and Higashiyama, T. (2017) pKAMA-ITACHI vectors for highly efficient crispr/cas9-mediated gene knockout in *Arabidopsis thaliana*. Plant Cell Physiol. 58: 46-56. https://doi.org/10.1093/pcp/pcw191.

Turunen, J.J., Niemelä, E.H., Verma, B. and Frilander, M.J. (2013) The significant other: splicing by the minor spliceosome. Wiley Interdiscip. Rev. RNA 4: 61-76. https://doi.org/10.1002/wrna.1141.

Wilkinson, M.E., Charenton, C. and Nagai, K. (2020) RNA splicing by the spliceosome. Annu. Rev. Biochem. 89: 359-388. https://doi.org/10.1146/annurev-biochem-091719-064225.

Zhan, X., Yan, C., Zhang, X., Lei, J. and Shi, Y. (2018) Structures of the human pre-catalytic spliceosome and its precursor spliceosome. Cell Res. 28: 1129-1140. https://doi.org/10.1038/s41422-018-0094-7.

Table 1

Gene	difference of percentage of intron retention	log(fold change)	FDR	Gene function
AT4G15802	46.4	−1.01	1.07×10^{-92}	Heat shock factor binding protein
AT2G39080	64.0	−1.54	2.64×10^{-71}	NAD(P)-binding Rossmann-fold superfamily protein
AT5G22650	64.5	−1.55	7.89×10^{-71}	Histone deacetylase 2B (HD2B)
AT4G13615	39.7	−0.85	1.46×10^{-69}	Uncharacterised protein family SERF
AT3G54670	90.2	−3.23	4.18×10^{-67}	Structural maintenance of chromosomes family protein (SMC1)
AT1G80500	44.1	−0.96	2.21×10^{-55}	SNARE-like superfamily protein
AT2G16485	78.2	−2.21	2.08×10^{-54}	NEEDED FOR RDR2-INDEPENDENT DNA METHYLATION (NERD)
AT4G05050*	15.1	−6.28	1.58×10^{-52}	ubiquitin 11
AT3G22880*	73.4	−1.94	1.66×10^{-52}	DNA repair (Rad51) family protein (DMC1)
AT3G51460	41.2	−0.88	2.01×10^{-49}	Phosphoinositide phosphatase family protein
AT5G27380	57.3	−1.34	1.71×10^{-48}	Glutathione synthetase 2 (GSH2)
AT2G39960	48.5	−1.07	2.36×10^{-47}	Microsomal signal peptidase 25 kDa subunit (SPC25)
AT3G50590	66.6	−1.65	9.18×10^{-46}	Transducin/WD40 repeat-like superfamily protein
AT4G38240	76.9	−2.10	4.06×10^{-45}	α-1,3-mannosyl-glycoprotein β-1,2-N-acetylglucosaminyltransferase, putative
AT1G29940	76.9	−2.09	1.03×10^{-44}	Nuclear RNA polymerase A2 (NRPA2)
AT3G53180	79.4	−2.23	2.45×10^{-43}	Glutamate-ammonia ligases
AT5G22110	83.3	−2.56	6.78×10^{-42}	DNA polymerase epsilon subunit B2 (DPB2)
AT2G40840	29.1	−0.61	2.81×10^{-41}	Disproportionating enzyme 2 (DPE2)
AT3G62830	38.2	−0.82	2.30×10^{-40}	NAD(P)-binding Rossmann-fold superfamily protein
AT2G47650	42.6	−0.92	3.57×10^{-40}	UDP-glucuronic acid decarboxylase 4 (UXS4)
AT5G03740	38.5	−0.83	1.69×10^{-38}	Histone deacetylase 2C (HD2C)
AT3G51120	82.6	−2.62	8.62×10^{-38}	Zinc finger CCCH domain-containing protein 44
AT1G31660	64.1	−1.57	3.12×10^{-37}	Unknown protein
AT5G38380	65.5	−1.62	2.11×10^{-36}	Unknown protein
AT5G56900	59.4	−1.38	3.19×10^{-34}	CwfJ-like family protein/zinc finger (CCCH-type) family protein
AT5G44200	49.9	−1.14	2.70×10^{-32}	CAP-binding protein 20 (CBP20)
AT5G18410	70.4	−1.76	1.07×10^{-31}	Transcription activators
AT3G21215	49.8	−1.12	5.01×10^{-29}	RNA-binding (RRM/RBD/RNP motifs) family protein
AT1G24050	15.8	−0.32	1.85×10^{-28}	RNA-processing, Lsm domain
AT5G60150*	90.8	−3.05	3.74×10^{-28}	Unknown protein
AT1G29630	84.7	−2.72	5.32×10^{-27}	5″-3' Exonuclease family protein (EXO1)
AT1G63640*	49.6	−1.11	7.41×10^{-27}	P-loop nucleoside triphosphate hydrolases superfamily protein with CH (Calponin Homology) domain
AT1G06720	37.3	−0.80	2.33×10^{-26}	P-loop containing nucleoside triphosphate hydrolases superfamily protein

Gene	difference of percentage of intron retention	log(fold change)	FDR	Gene function
AT1G77320	75.4	−2.27	8.58×10^{-26}	Transcription coactivators
AT1G67960	66.5	−1.72	2.53×10^{-25}	Unknown protein
AT3G06820	67.8	−1.78	3.09×10^{-25}	Mov34/MPN/PAD-1 family protein
AT5G63700	86.1	−3.62	3.89×10^{-25}	Zinc ion binding/DNA binding protein
AT3G53520	23.5	−0.48	5.88×10^{-25}	UDP-glucuronic acid decarboxylase 1 (UXS1)
AT2G44270	37.5	−0.80	8.88×10^{-24}	Repressor of *lrx1* (ROL5)
AT3G24100	8.0	−0.16	2.29×10^{-22}	Uncharacterised protein family SERF
AT3G56900*	32.7	−0.69	2.46×10^{-22}	Transducin/WD40 repeat-like superfamily protein
AT2G27840	16.1	−0.32	2.48×10^{-22}	Histone deacetylase 2D (HD2D)
AT2G27170*	38.2	−0.81	8.54×10^{-22}	Structural maintenance of chromosomes (SMC) family protein
AT5G08430	65.4	−1.85	2.60×10^{-19}	SWIB/MDM2 and Plus-3 and GYF domain-containing protein
AT1G73350	48.9	−1.22	2.89×10^{-19}	Unknown protein
AT1G26170	48.3	−1.06	2.41×10^{-18}	ARM repeat superfamily protein
AT1G02750	43.0	−0.94	5.44×10^{-18}	Drought-responsive family protein
AT1G80210	54.2	−1.23	1.07×10^{-17}	Mov34/MPN/PAD-1 family protein
AT1G54370	51.4	−1.17	1.11×10^{-17}	Na^+/H^+ exchanger 5 (NHX5)
AT5G26990*	45.7	−1.04	3.94×10^{-17}	Drought-responsive family protein
AT1G04130*	31.1	−0.65	1.88×10^{-16}	Tetratricopeptide repeat (TPR)-like superfamily protein
AT4G24900	55.6	−5.64	1.99×10^{-16}	C2H2-domain protein (TTL)
AT1G79610	54.4	−1.25	6.55×10^{-16}	Na^+/H^+ exchanger 6 (NHX6)
AT4G30900	48.5	−1.08	1.57×10^{-13}	DNAse I-like superfamily protein
AT3G05700*	39.0	−0.84	3.11×10^{-12}	Drought-responsive family protein
AT2G47500*	22.7	−0.46	3.18×10^{-10}	P-loop nucleoside triphosphate hydrolases superfamily protein with CH (Calponin Homology) domain
AT1G56280*	5.4	−0.11	1.23×10^{-9}	drought-induced 19
AT3G04820*	20.9	−0.43	5.03×10^{-9}	Pseudouridine synthase family protein
AT5G24450*	25.0	−0.53	5.40×10^{-7}	Transcription factor IIIC, subunit 5
AT5G49230*	16.2	−0.34	0.00171	Drought-responsive family protein

* indicates the genes in the red square in Figure 2B

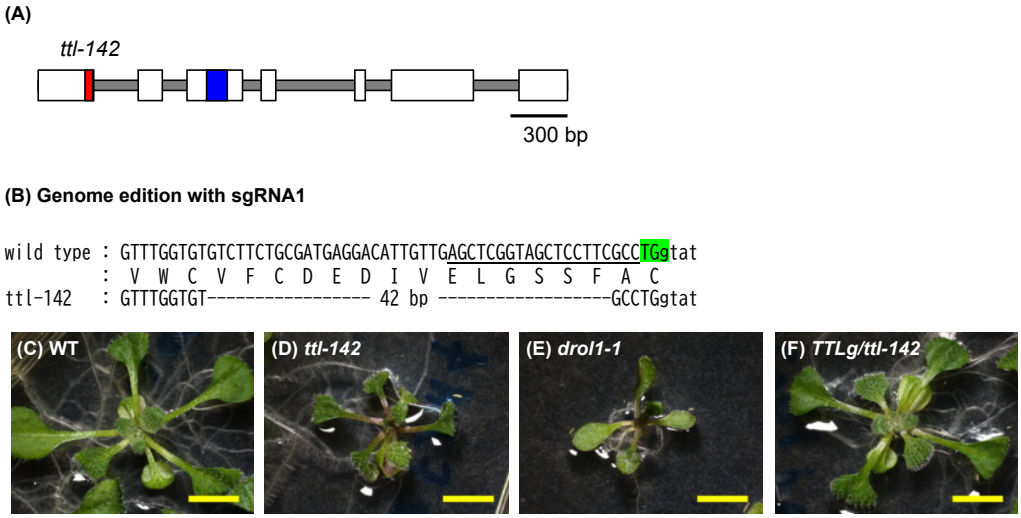

Figure 1

(A) Structure of *TTL*. Gray and white boxes indicate introns and exons, respectively. The blue box indicates the AT–AC intron present in exon 3, while the red box indicates the *ttl-142* mutation. (B) Nucleotide sequences surrounding TTL DNA targeted for genome editing. The WT nucleotide sequence and the corresponding deduced amino acid sequence are displayed in the first and second lines, respectively. The sgRNA target sequence is underlined, and the proto-spacer adjacent motif is colored green. Exons and introns are shown in uppercase and lowercase letters, respectively. The nucleotide sequences of alleles created by genome editing are shown below the WT. The numbers within the sequence indicate the length of deleted nucleotide sequences. Images for (C) WT, (D) *ttl-142*, (E) *drol1-1*, (F) *TTLg/ttl-142*. All photographs were taken 13 days after germination. Scale bar = 5 mm.

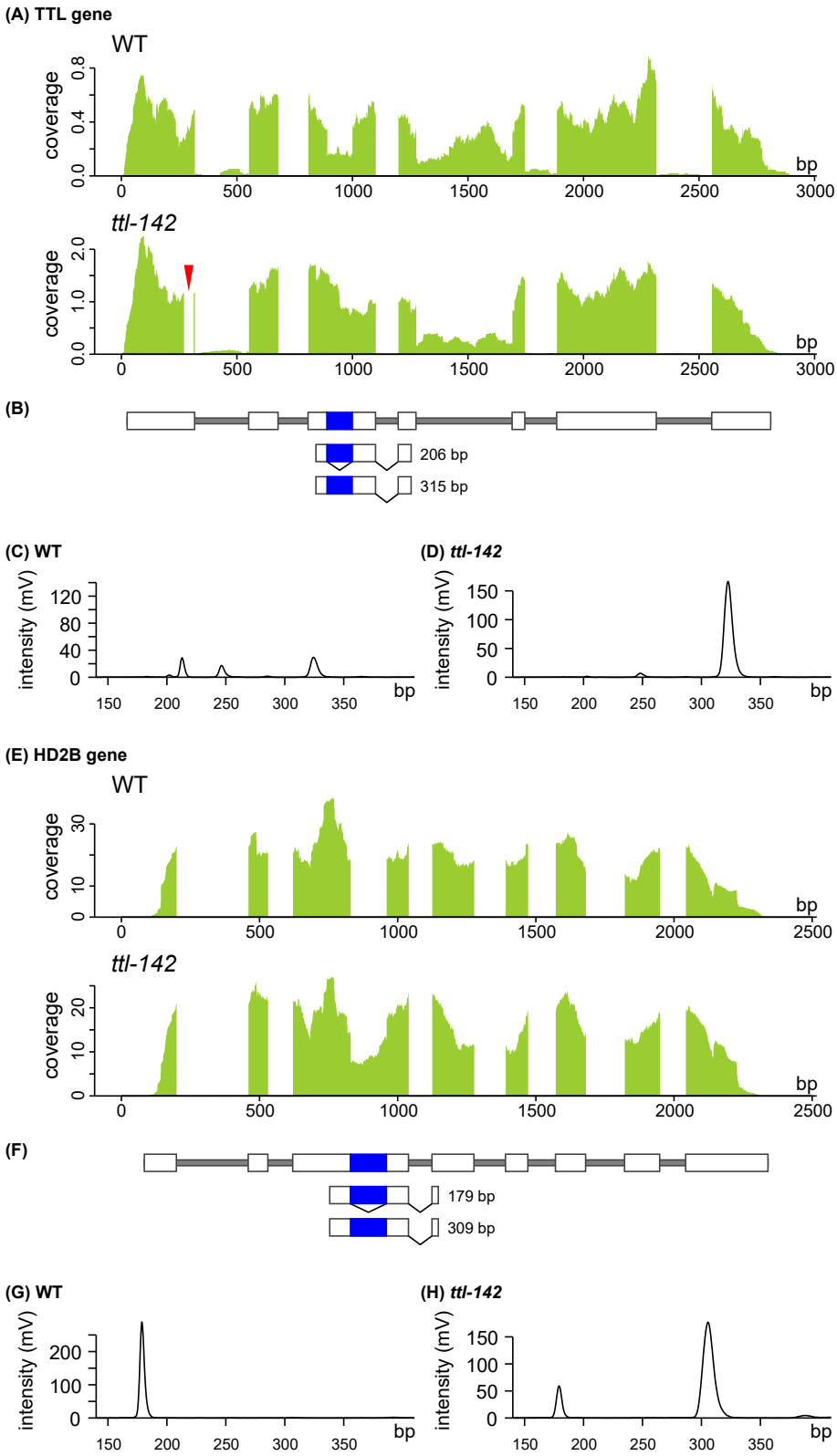

Figure 2

RNA-Seq and RT-PCR analyses of retention of the AT–AC intron of TTL and HD2B in the wild type and *ttl-142* mutant. (A) RNA-Seq analysis of *TTL*. Total RNA was extracted from three-day-old WT (upper) and *ttl-142* (lower) seedlings that were then subjected to cDNA library construction for next-generation sequencing. All reads obtained were aligned to the *TTL* gene sequence. The x-axis represents reference sequences, while the y-axis indicates short read coverage. The red arrowhead indicates the deletion in *ttl-142*. (B) Gene structure of *TTL*. Gray and white boxes represent introns and exons, respectively. Blue boxes indicate the AT–AC-type

introns. Expected RT-PCR products in (C, D) are also indicated, along with their size. (C, D) Chip electrophoresis of DNA fragments amplified by RT-PCR from (C) WT and (D) *ttl-142* RNA. The x-axis represents DNA size in bp, and the y-axis indicates fluorescence intensity corresponding to DNA abundance. (E-H) Similar experiment performed for HD2B.

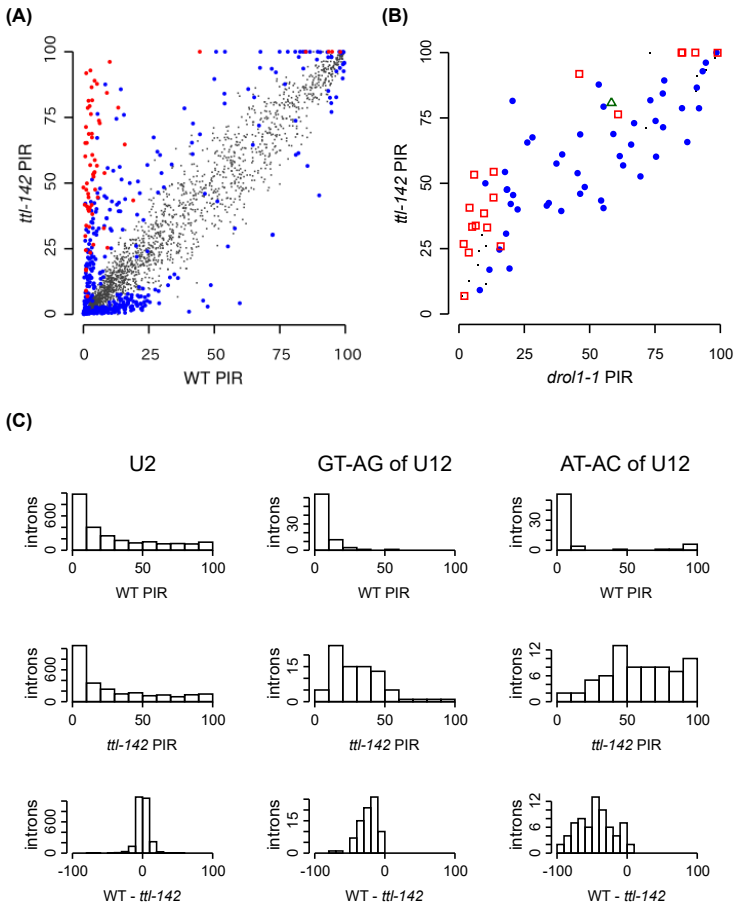

Figure 3

Global intron retention for the *ttl-142* mutant. (A) Scatter plot of the percentage of intron retention (PIR) for the WT and *ttl-142* mutant. Small and large dots represent 2,329 introns analyzed by ASpli (Estefania et al., 2021). AT–AC introns and other intron types (i.e., mainly GT–AG) with FDR <0.01 are plotted as large red and blue dots, respectively. (B) Comparison of PIR between *ttl-142* and *drol1-1*. PIR values for all AT–AC introns in *ttl-142* and *drol1-1* were plotted on the vertical and horizontal axes, respectively. Red squares, green triangles, and large blue dots represent AT–AC introns with FDR values (compared to the WT) that were <0.01 in the *ttl-142*, *drol1-1*, and both mutants, respectively. Small dots represent other AT–AC introns. (C) Histogram of PIR values. The left to right columns depict the counts of U2 introns, GT–AG introns in U12 and AT–AC introns in U12 grouped by PIR. The first and second rows represent observed PIR values for the WT and *ttl-142*, respectively. The third row represents differences in PIR (i.e., *ttl-142* subtracted from Col) between WT and *ttl-142*.

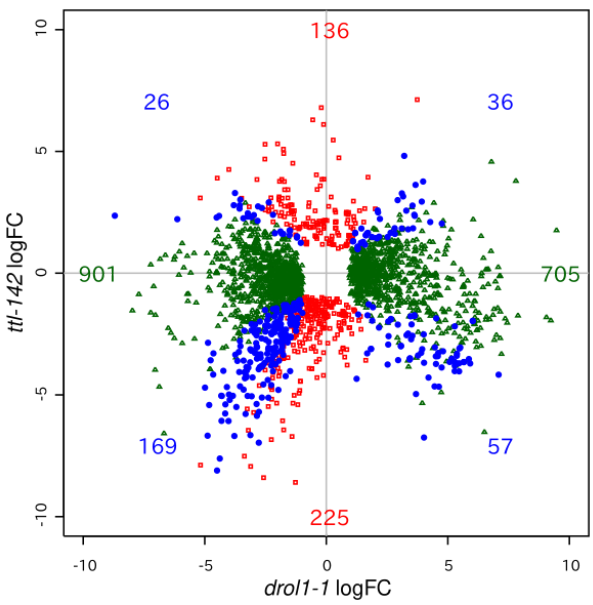

Figure 4

Comparison of differentially expressed genes in *ttl-142* and *drol1-1*. Log-fold changes in gene expression levels in *ttl-142* and *drol1-1* were plotted on the vertical and horizontal axes, respectively. Red squares, green triangles, and blue dots represent genes with FDRs less than 1×10^{-4} in the *ttl-142*, *drol1-1*, and both mutants, respectively. Numbers in the plots represent the number of genes in each group.

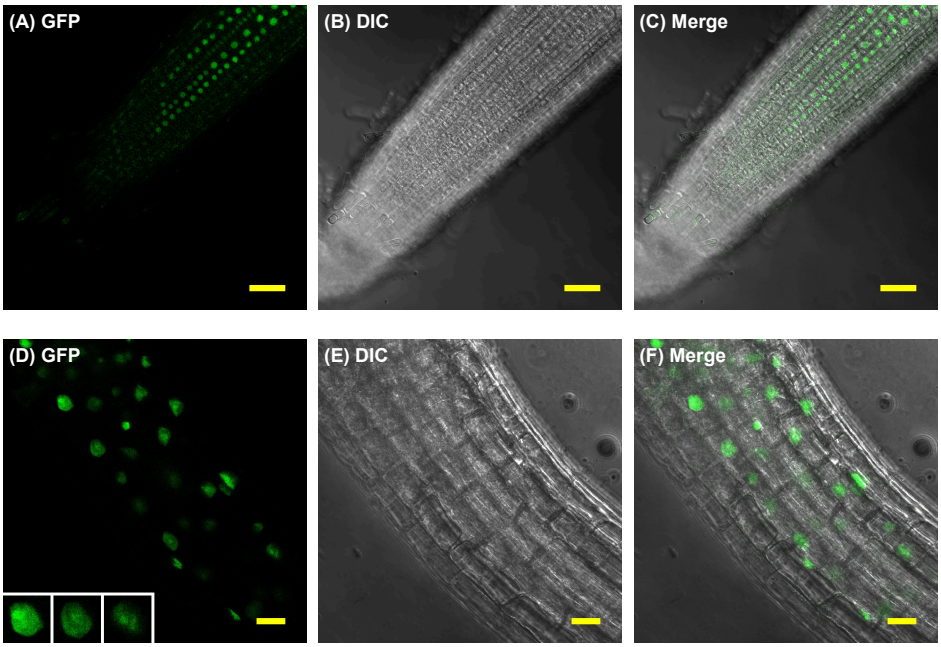

Figure 5

Intracellular localization of TTL in plant root cells. (A-C) Root tip of a WT transformant that expressed TTLmmI-G3GFP. Shown are (A) A fluorescent image due to TTLmmI-G3GFP, (B) a differential interference contrast image, and (C) a merged image. Scale bar = 50 μm. (D-F) A magnified image of a different root. Enlarged images of several nuclei are shown in the inset of (D). Scale bar = 20 μm. All images were taken using an LSM 710 AxioObserver (Zeiss, Jena, Germany).